

Second order resonant Raman scattering in single layer tungsten disulfide (WS_2)

A. A. Mitiglu,^{1,2} P. Plochocka,¹ G. Deligeorgis,³ S. Anghel,^{2,4} L. Kulyuk,² and D. K. Maude¹

¹LNCMI, CNRS-UJF-UPS-INSA, Grenoble and Toulouse, France

²Institute of Applied Physics, Academiei Str. 5, Chisinau, MD-2028, Republic of Moldova

³FORTH-IESL, Microelectronics Research Group, P.O. Box 1527, 71110 Heraklion, Crete, Greece

⁴Ruhr-Universität Bochum, Anorganische Chemie III, D-44801 Bochum Germany

(Dated: June 30, 2014)

Resonant Raman spectra of single layer WS_2 flakes are presented. A second order Raman peak (2LA) appears under resonant excitation with a separation from the E_{2g}^1 mode of only 4cm^{-1} . Depending on the intensity ratio and the respective line widths of these two peaks, any analysis which neglects the presence of the 2LA mode can lead to an inaccurate estimation of the position of the E_{2g}^1 mode, leading to a potentially incorrect assignment for the number of layers. Our results show that the intensity of the 2LA mode strongly depends on the angle between the linear polarization of the excitation and detection, a parameter which is neglected in many Raman studies.

I. INTRODUCTION

Single layer transition metal dichalcogenides (TMDs) are a class of emerging nano-materials which have recently become the subject of intense investigation, in part due to their truly two-dimensional character and due to the wealth of applications that may benefit from their unique characteristics. In TMDs, a single layer is composed of a monolayer of the transition metal with a chalcogen monolayer above and below. The intra layer coupling is strong due to the chalcogen metal covalent bonds. The electronic properties of a single layer are significantly different from bulk crystals, where the stacked layers are coupled by weak Van der Waals forces. Bulk TMDs are semiconductors with an indirect gap in the near infrared spectral range. In contrast, single layer TMDs, such as molybdenum disulfide (MoS_2), tungsten disulfide (WS_2) or tungsten diselenide (WSe_2), are two dimensional (2D) semiconductors with a *direct gap in the visible spectral range* with a large number of potential applications in optoelectronics.¹⁻⁹

Many experimental techniques have been employed to study the electronic properties of layered materials. Among them, Raman spectroscopy, has been extensively used to determine the number of layers in TMDs^{5,7,10-12} and in graphene.^{13,14} The vibrational spectra are sensitive to the thickness of the crystal so that small changes in the separation of first order Raman modes can be used to differentiate between bulk, monolayer, bilayer and tri-layer crystals. In transition metal dichalcogenides, the excitation of Raman modes can easily be tuned to coincide with one of the direct optical transitions. Indeed, the large number of transitions (excitons A,B and C), which are often fortuitously close to laser lines commonly used, means that Raman data is often taken close to resonant conditions. In turn this can result in additional and frequently unwanted complications when interpreting the data.

Resonant Raman spectra are composed of both first and second order Raman excitations, as demonstrated for bulk MoS_2 ^{15,16} or WS_2 .¹⁷⁻¹⁹ Recently, second or-

der Raman modes have been reported in single layer WS_2 ,²⁰⁻²³ MoS_2 ²⁴, TaSe_2 ²⁵ and WSe_2 .²⁶ Such resonant vibrational spectra can provide significant additional information concerning the electronic properties. For example, it has been suggested that the observation of a strong second order Raman resonance involving the longitudinal acoustic phonons (2LA) in monolayer WS_2 is a signature of the single layer nature of the sample.²⁰

Nevertheless, the resonant Raman spectra in atomically thin TMDs are relatively unexplored and far from being fully understood. In monolayer WSe_2 , an additional Raman mode, separated by only a few cm^{-1} from the E_{2g}^1 and A_{1g} modes, and whose origin remains to be elucidated, was recently reported.²⁶ From a fundamental physics point of view, the inter valley scattering process involving the 2LA phonon was suggested to be the main source of valley depolarization.²⁷ For all these reasons, understanding the resonant Raman processes in TMDs is of great importance.

In this paper, we present resonant Raman scattering measurements performed on a single layer of tungsten disulphide. We focus on the second order Raman resonance involving the longitudinal acoustic phonon (2LA), which is separated by only 4cm^{-1} from the E_{2g}^1 mode. We show that due to their small separation, the two modes can be undistinguishable, leading to an erroneous estimation of the separation of the E_{2g}^1 and A_{1g} modes, which is normally accepted to be a robust indication of the crystal thickness. Crucially, measurements involving linear polarization show that depending on the angle between polarization of the excitation and detection the 2LA mode can even dominate over the E_{2g}^1 mode or vice versa. In most Raman measurements performed to characterize samples, the polarization of the excitation and detection is unknown so that incorrect conclusions concerning the number of the layers present can easily be reached.

II. EXPERIMENTAL TECHNIQUES

Single bulk crystal of 2H-WS₂ (the hexagonal 2H-polytype of tungsten disulphide) have been grown using chemical vapor transport with Bromine as the transport agent.²⁸ Single layer flakes of tungsten disulfide have been obtained from these crystals using mechanical exfoliation. For the measurements, the sample was placed in a helium flow cryostat with optical access. The μ -Raman measurements have been performed in the back scattering configuration. Excitation and collection was implemented using a microscope objective with a numerical aperture $NA = 0.66$ and magnification $50\times$. The typical diameter of the laser spot was approximately $1\mu\text{m}$. The μ -Raman spectra have been recorded using a spectrometer equipped with a CCD camera and a green solid-state laser, emitting at 532 nm , was used for excitation.

III. RESONANT RAMAN SCATTERING

The 2H-WS₂ crystal belongs to D_{6h}^4 space group. Of the 12 first order phonon modes at the Brillouin zone center four are Raman active: A_{1g} , E_{1g} , E_{2g}^1 and E_{2g}^2 . In the back scattering configuration, the E_{1g} mode is forbidden, and the E_{2g}^2 mode is observed only in the very low frequency region.¹⁹ In addition, E_{2g}^2 is a shared mode originating from the relative motion of the atoms in different layers, and is thus absent in single layer samples. As a result, the Raman spectra of a single layer WS₂ are dominated by two first order modes: E_{2g}^1 , which is associated with the in plane motion of the sulfur and tungsten atoms in opposite directions and A_{1g} , which is associated with the out of plane motion of the sulfur atoms.¹⁹ In bulk WS₂, the separation between these two modes is 66cm^{-1} and it decreases gradually with the number of layers reaching 62cm^{-1} for a single layer.^{5,6,20,22,23}

A. Room temperature

A typical resonant Raman spectrum taken at 300K is presented in Fig 1(a). Two strong features are observed. A single resonance peak at 417 cm^{-1} , which corresponds to the A_{1g} mode in single layer of tungsten disulphide,^{5,6,20,22,23} together with a more complicated feature observed around 353 cm^{-1} . It is composed of two features; a peak at 351 cm^{-1} accompanied by a weaker peak at 355 cm^{-1} corresponding to the E_{2g}^1 mode in single layer WS₂.^{5,6,20,22,23} The separation between A_{1g} and E_{2g}^1 of 62cm^{-1} proves the single layer character of our sample. The presence of an additional peak on the low frequency side of the E_{2g}^1 mode has been reported for bulk crystals¹⁷⁻¹⁹ and very recently for single layer WS₂.^{20,22} This additional peak has been assigned to a second order Raman resonance involving longitudinal acoustic phonons (2LA).^{17-20,22} The peak we observe

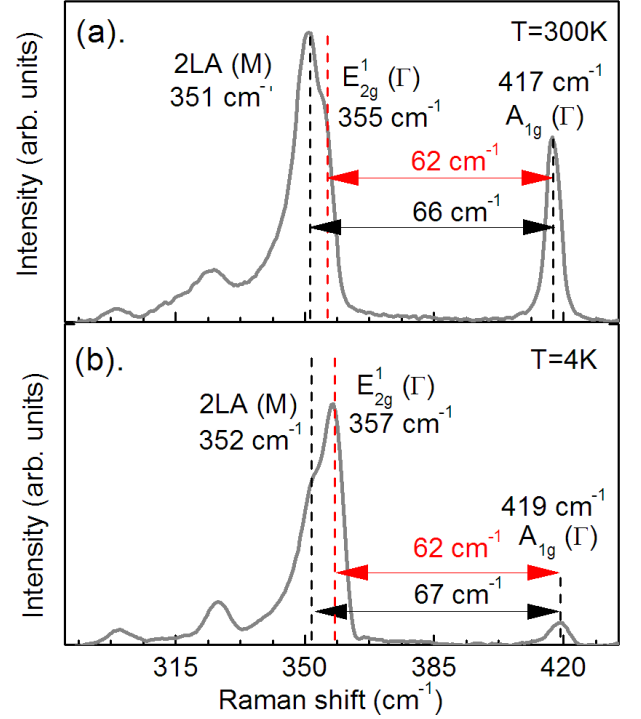


FIG. 1. (color online) (a), (b) Typical μ Raman spectra measured at $T = 300$ and $T = 4\text{K}$. The dashed lines indicate the position of three Raman modes: 2LA, E_{2g}^1 and A_{1g} .

at 351 cm^{-1} corresponds well to such a second order Raman resonance. Our data suggests, in apparent agreement with calculations and measurements presented by Berkdemir et al.,²⁰ that the 2LA mode is stronger than E_{2g}^1 mode for single layer material. We will see later that this agreement is fortuitous since the angle of the linear polarization between excitation and detection is completely unknown in our measurements.

B. Low temperature

Further proof of the 2LA character of the peak at 351 cm^{-1} is provided by measurements at low temperature ($T = 4\text{K}$) presented in Fig 1(b). Compared to the Raman data measured at 300K , a small blue shift of the resonance frequencies is observed with decreasing temperature due to the anharmonic vibrations in the lattice in the interatomic potential energy mediated by phonon - phonon interactions^{29,30}. However, the dominant effect of the temperature is the radical change in the intensity ratio between the E_{2g}^1 and 2LA modes. At room temperature the 2LA mode dominates over the E_{2g}^1 while at low temperature the situation is reversed. As the 2LA mode is an overtone its temperature dependence is expected to take the form $[n(\omega_1, T) + 1] \times [n(\omega_2, T) + 1]$, where $n(\omega, T) = (\exp(\frac{\hbar\omega}{kT}) - 1)^{-1}$ is the phonon occupa-

tion number for a process in which phonons with frequencies ω_1, ω_2 are absorbed and created respectively.¹⁵ A quick estimation using the frequency of 2LA mode shows that its intensity should decrease by 1.5 times between room temperature and 4K. This estimation is in a good agreement with our data with the assumption that the intensity of the E_{2g}^1 mode is rather insensitive to temperature.¹⁸ Our data is clearly not consistent with the assignment of the 351 cm^{-1} feature to a combination process whose temperature dependence would take the form $n(\omega_1, T) \times [n(\omega_2, T) + 1]$.¹⁵ In such a scenario the resonance would simply vanish at 4K. The temperature dependence of the intensity of this resonance is therefore an independent proof of its 2LA character. We note that the variation of the direct gap with temperature could detune the resonant excitation and also in principle contribute to a decrease of the intensity of the 2LA resonance. However, the phonon occupation is expected to dominate the temperature dependence.

C. Assigning layer thickness

Let us now focus on the separation between these three resonances. Regardless of the temperature, the separation between A_{1g} and E_{2g}^1 is 62 cm^{-1} and the separation between A_{1g} and 2LA is 66 cm^{-1} . However, the separation between the 2LA and E_{2g}^1 modes is only 4 cm^{-1} so that, any broadening of the peaks due to impurities/defects in the sample or simply a lack of resolution might lead to an incorrect determination of the frequency of the E_{2g}^1 mode. As a result, the separation between A_{1g} and E_{2g}^1 might be overestimated, in turn leading to an overestimation of the number of layers in the sample. To illustrate the universality of this problem, we have measured Raman spectra for several single layer flakes in order to analyze the separation $\Delta\omega$ between different Raman features. The summary of such an analysis is presented in Fig 2. The symbols correspond to the three different combinations: $\Delta\omega_1 = \omega(A_{1g}) - \omega(2LA)$, $\Delta\omega_2 = \omega(A_{1g}) - (\omega(2LA) + \omega(E_{2g}^1))/2$ and $\Delta\omega_3 = \omega(A_{1g}) - \omega(E_{2g}^1)$ respectively. The latter is generally used in the literature to determine the number of layers present. For comparison, the literature values for the separation between (A_{1g} and E_{2g}^1 for single, bi-, tri-layer and bulk^{6,20,31} are indicated by broken lines.

The Raman splitting $\Delta\omega_3$ is generally considered to be a robust signature of the number of the layers in the sample. For our data, in which E_{2g}^1 and 2LA are clearly resolved, for all the flakes, $\Delta\omega_3$ is equal to 62 cm^{-1} , demonstrating the single layer character of our flakes.^{6,20,31} However, if the modes E_{2g}^1 and 2LA are not well resolved, in any analysis which neglects the possible presence of the 2LA mode the assignment of the number of layers becomes highly problematic. If the 2LA mode dominates over E_{2g}^1 the measured difference will correspond to the $\Delta\omega_1 = \omega(A_{1g}) - \omega(2LA)$ which is approximately

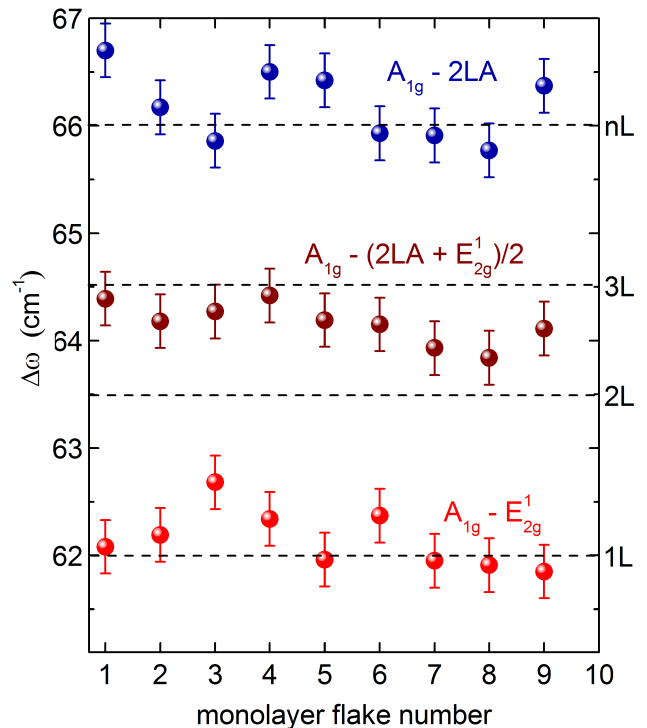


FIG. 2. (color online) The symbols indicate the frequency difference $\Delta\omega$ between: A_{1g} and 2LA, between A_{1g} and the average frequency of 2LA and E_{2g}^1 , and between A_{1g} and E_{2g}^1 . The dashed lines indicate the accepted values for the separation of A_{1g} and E_{2g}^1 for single, bi-, tri-layer and bulk.^{6,20,31}

66 cm^{-1} , leading to the incorrect assignment of Raman from a bulk sample.^{17–19} On the other hand, if the intensity of 2LA and E_{2g}^1 modes are similar, the frequency of the Raman features will correspond to the average of the two peaks. The measured frequency difference $\omega(A_{1g}) - (\omega(2LA) + \omega(E_{2g}^1))/2 \simeq 64\text{ cm}^{-1}$ then correspond to the bi- or tri-layer system.^{6,20,31} This poses a significant problem for the correct assignment of the number of layers especially since the relative intensity between E_{2g}^1 and 2LA depends on several parameters, including the temperature and the excitation wavelength (2LA is only observed for resonant excitation) as shown for bulk crystals.^{17,18} In the following, we show that the relative linear polarization of the excitation and detection also significantly influences this intensity ratio.

D. Polarization dependence

μ -Raman spectra have been measured at $T = 4.2\text{ K}$ as a function of the relative angle θ between the linearly polarized excitation and the emission. We have performed measurements when the linear polarization of the excitation was fixed and the angle was varied in the detection and vice versa. We have verified that the results are only dependent on the angle θ ; the same spectra are always

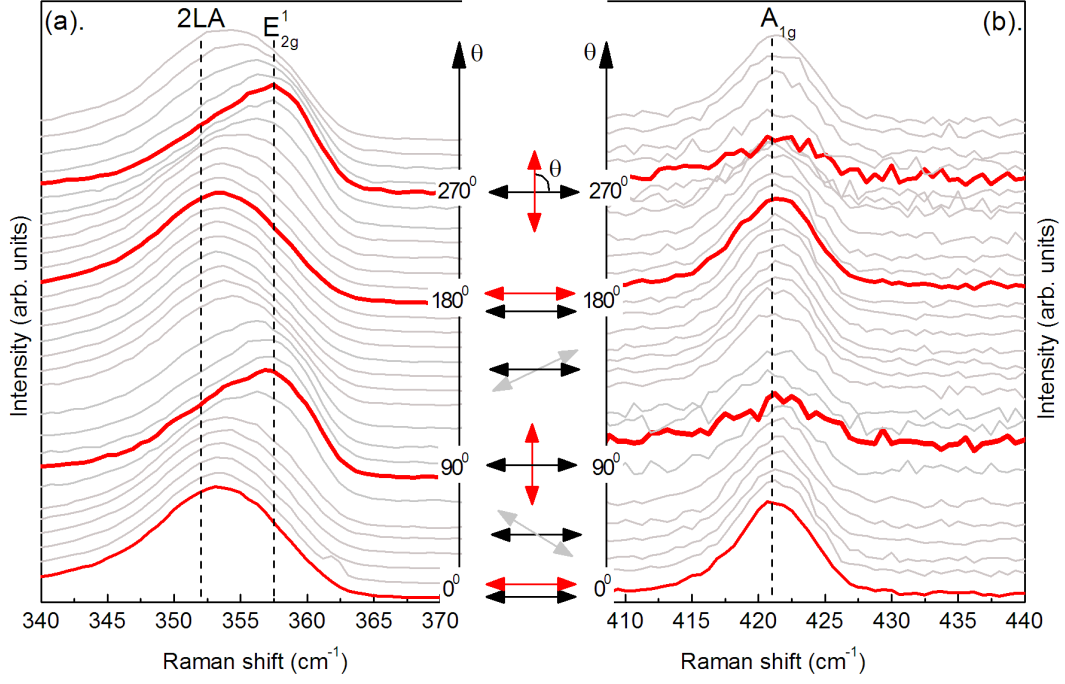


FIG. 3. (color online) Typical results are presented in (a) for the frequency region corresponding to the 2LA and E_{2g}^1 modes and in (b) for the A_{1g} mode. The spectra for different angles θ are vertically shifted for clarity. The spectra for co and cross polarized configuration are indicated by thick red lines. The orientation of the detection (red arrows) and excitation (black arrows) linear polarization are indicated for the co and cross polarization configuration.

observed for co and cross linearly polarized beams independently of the angle of the linear polarization with respect to the sample. Typical results are presented in Fig 3(a) for frequencies in the region corresponding to the 2LA and E_{2g}^1 modes and in Fig 3(b) for the A_{1g} mode. The spectra for different angles are shifted vertically for clarity. The spectra for co and cross polarized configuration are indicated by thick red lines. The intensity of the 2LA mode changes as a function of the angle θ . When the polarization of the excitation and detection are orthogonal, the intensity of 2LA phonon resonance reaches a minimum. For parallel configuration the 2LA mode is stronger than E_{2g}^1 . For angles $0 < \theta < 90$ degrees the intensity of 2LA mode changes gradually. A similar behavior is observed for A_{1g} mode while the intensity of E_{2g}^1 is constant within experimental error.

The intensities of the Raman peaks as a function of the angle between polarization of the excitation and detection are presented in Fig 4. The linear polarization in detection was fixed, either horizontal or vertical as indicated by the red arrows on Fig 4(a)-(b). The polarization of the excitation was then rotated through 180° . The co and cross polarized configurations are indicated by the arrows in Fig 4(a)-(b). The black arrow represent the orientation of the polarization of the excitation. The data obtained for horizontal and vertical configurations are presented in Fig 4(a)-(b) respectively. The experi-

mental values of the intensity of 2LA and A_{1g} modes are indicated by symbols. The data is well described by a sinusoidal function (solid line). The minimum of the intensity of both modes for horizontally polarized detection is shifted by 90 degrees with respect to the results for the vertically polarized detection. This proves that the ratio between 2LA and E_{2g}^1 depends only on the angle θ between the excitation and detection polarization. For the A_{1g} mode the oscillation of the intensity as a function of the angle θ , as well as the lack of intensity changes of E_{2g}^1 (not shown) is understood and comes from the form of Raman tensors.³² The analysis for the 2LA mode is not as straight forward as that of the A_{1g} , since the 2LA mode arises from a double resonance process. However, it is experimentally well established that the A_{1g} and 2LA modes have the same polarization dependence. For example, the polarization characteristic of 2LA mode has been determined in bulk crystals¹⁷⁻¹⁹ where it was compared with the results of neutron scattering where the phonon dispersion along crystal axis was measured in the same plane as the polarization of the light. As already demonstrated by Chen *et al.*³³ a single layer, exhibits the same polarization characteristic.

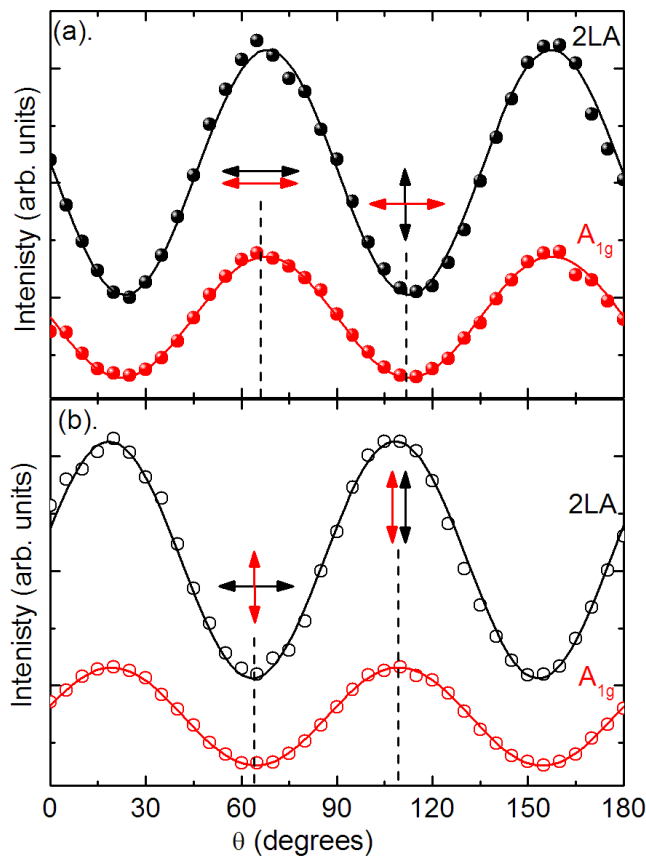


FIG. 4. (color online) Intensity of the 2LA and A_{1g} modes (symbols). (a), (b) represent two different experimental configurations; the linear polarization in detection was either horizontal or vertical as indicated by the red arrows. The black arrows indicated the excitation polarization in the co and crossed configurations

E. Raman modes at lower energies

Finally, we will discuss the two Raman modes with low intensity observed at ~ 300 and ~ 320 cm^{-1} in Fig.1(a-b). They have been contradictorily linked to the monolayer or multilayer nature of the flake studied.^{20,34} We have investigated a large number of samples and these

modes are present in all investigated flakes which show single layer character. They could be assigned to 2LA modes with a wave vector in the vicinity of the K point in the Brillouin zone as suggested for bulk crystals.¹⁷ An alternative assignment would be the E_{1g} mode, which in bulk crystals is not allowed in the back scattering (reflection) geometry. Certainly, this controversy shows that resonant Raman spectroscopy is far from being fully understood in single layer dichalcogenides.

IV. CONCLUSION

To summarize, under resonant excitation, the presence of the 2LA Raman mode complicates the determination of the number of layers in WS_2 flakes. Thankfully, the assignment of a monolayer from the E_{2g}^1 - A_{1g} separation remains robust. However, mono layers can be incorrectly assigned to bi-layer, tri-layer or even bulk crystals depending on the intensity of the 2LA mode. All our data has been taken using 532nm excitation, nevertheless, our conclusions should apply to other excitation wavelengths. Sourisseau *et al.*^{17,18} studied in detail the dependence of the intensity of 2LA mode as a function of excitation wavelength. They have shown, that whenever the laser is in resonance with the excitonic transition (A,B or C) both the 2LA and the A_{1g} modes are enhanced. Thus, our conclusions and analysis will be valid whenever the 2LA mode is present in the Raman spectrum, in other words whenever the laser is in resonance with one of the excitonic transitions. The evolution of the intensity ratio of the 2LA and E_{2g}^1 - A_{1g} modes with polarization prescribes using the intensity of the 2LA mode to identify a monolayer, unless the polarization angle between excitation and detection is carefully controlled, which is rarely the case. As many Raman characterizations are frequently performed close to resonant excitation, and without controlling the polarization angle, considerable care should be exercised when analyzing these spectra.

ACKNOWLEDGMENTS

This work was partially supported by Programme Investissements d'Avenir under the program ANR-11-IDEX-0002-02 - reference ANR-10-LABX-0037-NEXT, ANR JCJC project milliPICS, the Region Midi-Pyrénées under contract MESR 13053031 and STCU project 5809.

¹ K. F. Mak, C. Lee, J. Hone, J. Shan, and T. F. Heinz, *Phys. Rev. Lett.* **105**, 136805 (2010).

² A. Splendiani, L. Sun, Y. Zhang, T. Li, J. Kim, C.-Y. Chim, G. Galli, and F. Wang, *Nano Letters* **10**, 1271 (2010), pMID: 20229981, <http://pubs.acs.org/doi/pdf/10.1021/nl903868w>.

³ G. Eda, H. Yamaguchi, D. Voiry, T. Fujita, M. Chen, and M. Chhowalla, *Nano Letters* **11**, 5111 (2011), <http://pubs.acs.org/doi/pdf/10.1021/nl201874w>.

⁴ K. Albe and A. Klein, *Phys. Rev. B* **66**, 073413 (2002).

⁵ H. R. Gutierrez, N. Perea-Lpez, A. L. Elas, A. Berkdemir, B. Wang, R. Lv, F. Lpez-Uras, V. H. Crespi, H. Terrones, and M. Terrones, *Nano Letters* **13**, 3447 (2013), <http://pubs.acs.org/doi/pdf/10.1021/nl3026357>.

⁶ W. Zhao, Z. Ghorannevis, L. Chu, M. Toh, C. Kloc, P.-H. Tan, and G. Eda, *ACS Nano* **7**, 791 (2013), <http://pubs.acs.org/doi/pdf/10.1021/nn305275h>.

- ⁷ Q. H. Wang, K. Kalantar-Zadeh, A. Kis, J. N. Coleman, and M. S. Strano, *Nature Nanotechnology* **7**, 699 (2012).
- ⁸ T. Cao, G. Wang, W. Han, H. Ye, C. Zhu, J. Shi, Q. Niu, P. Tan, E. W. B. Liu, and J. Feng, *Nature Communications* **3**, 887 (2012).
- ⁹ K. F. Mak, K. He, C. Lee, G. H. Lee, J. H. T. F. Heinz, and J. Shan, *Nature Materials* **12**, 207 (2013).
- ¹⁰ S.-L. Li, H. Miyazaki, H. Song, H. Kuramochi, S. Nakaharai, and K. Tsukagoshi, *ACS Nano* **6**, 7381 (2012), <http://pubs.acs.org/doi/pdf/10.1021/nn3025173>.
- ¹¹ C. Lee, H. Yan, L. E. Brus, T. F. Heinz, J. Hone, and S. Ryu, *ACS Nano* **4**, 2695 (2010), pMID: 20392077, <http://pubs.acs.org/doi/pdf/10.1021/nn1003937>.
- ¹² H. Li, G. Lu, Y. Wang, Z. Yin, C. Cong, Q. He, L. Wang, F. Ding, T. Yu, and H. Zhang, *Small* **9**, 1974 (2013).
- ¹³ A. C. Ferrari, J. C. Meyer, V. Scardaci, C. Casiraghi, M. Lazzeri, F. Mauri, S. Piscanec, D. Jiang, K. S. Novoselov, S. Roth, and A. K. Geim, *Phys. Rev. Lett.* **97**, 187401 (2006).
- ¹⁴ A. Gupta, G. Chen, P. Joshi, S. Tadigadapa, and Eklund, *Nano Letters* **6**, 2667 (2006), pMID: 17163685, <http://pubs.acs.org/doi/pdf/10.1021/nl061420a>.
- ¹⁵ J. Chen and C. Wang, *Solid State Communications* **14**, 857 (1974).
- ¹⁶ G. L. Frey, R. Tenne, M. J. Matthews, M. S. Dresselhaus, and G. Dresselhaus, *Phys. Rev. B* **60**, 2883 (1999).
- ¹⁷ C. Sourisseau, M. Fouassier, M. Alba, A. Ghorayeb, and O. Gorochoy, *Materials Science and Engineering: B* **3**, 119 (1989).
- ¹⁸ C. Sourisseau, F. Cruege, M. Fouassier, and M. Alba, *Chemical Physics* **150**, 281 (1991).
- ¹⁹ T. Sekine, T. Nakashizu, K. Toyoda, K. Uchinokura, and E. Matsuura, *Solid State Communications* **35**, 371 (1980).
- ²⁰ A. Berkdemir, H. R. Gutierrez, A. R. Botello-Mendez, N. Perea-Lpez, A. L. Elias, C.-I. Chia, B. Wang, V. H. Crespi, F. Lpez-Uras, J.-C. Charlier, H. Terrones, and M. Terrones, *Scientific Reports* **3**, 1755 (2013).
- ²¹ D. O. Dumcenco, Y.-C. Su, Y.-P. Wang, K.-Y. Chen, Y.-S. Huang, C.-H. Ho, and K.-K. Tiong, *Chinese Journal of Physics* **3**, 270 (2011).
- ²² J.-G. Song, J. Park, W. Lee, T. Choi, H. Jung, C. W. Lee, S.-H. Hwang, J. M. Myoung, J.-H. Jung, S.-H. Kim, C. Lansalot-Matras, and H. Kim, *ACS Nano* **7**, 11333 (2013), <http://pubs.acs.org/doi/pdf/10.1021/nn405194e>.
- ²³ H. Zeng, G.-B. Liu, J. Dai, Y. Yan, B. Zhu, R. He, L. Xie, S. Xu, X. Chen, W. Yao, and X. Cui, *Scientific Reports* **3**, 1608 (2013).
- ²⁴ H. Li, Q. Zhang, C. C. R. Yap, B. K. Tay, T. H. T. Edwin, A. Olivier, and D. Baillargeat, *Advanced Functional Materials* **22**, 1385 (2012).
- ²⁵ P. Hajiyev, C. Cong, C. Qiu, and T. Yu, *Scientific Reports* **3**, 2593 (2013).
- ²⁶ X. Luo, Y. Zhao, J. Zhang, M. Toh, C. Kloc, Q. Xiong, and S. Y. Quek, *Phys. Rev. B* **88**, 195313 (2013).
- ²⁷ G. Kioseoglou, A. T. Hanbicki, M. Currie, A. L. Friedman, D. Gunlycke, and B. T. Jonker, *Applied Physics Letters* **101**, 221907 (2012).
- ²⁸ A. A. Mitoglu, P. Plochocka, J. N. Jadcak, W. Escoffier, G. L. J. A. Rikken, L. Kulyuk, and D. K. Maude, *Phys. Rev. B* **88**, 245403 (2013).
- ²⁹ R. Yan, J. R. Simpson, S. Bertolazzi, J. Brivio, M. Watson, X. Wu, A. Kis, T. Luo, A. R. Hight Walker, and H. G. Xing, *ACS Nano* **8**, 986 (2014), <http://pubs.acs.org/doi/pdf/10.1021/nn405826k>.
- ³⁰ N. A. Lanzillo, A. Glen Birdwell, M. Amani, F. J. Crowne, P. B. Shah, S. Najmaei, Z. Liu, P. M. Ajayan, J. Lou, M. Dubey, S. K. Nayak, and T. P. O'Regan, *Applied Physics Letters* **103**, 093102 (2013).
- ³¹ A. Molina-Sánchez and L. Wirtz, *Phys. Rev. B* **84**, 155413 (2011).
- ³² D. Loudon, *Adv. Phys.* **13**, 423 (1964).
- ³³ Y. Chen, D. O. Dumcenco, Y. Zhu, X. Zhang, N. Mao, Q. Feng, M. Zhang, J. Zhang, P.-H. Tan, Y.-S. Huang, and L. Xie, *Nanoscale* **6**, 2833 (2014).
- ³⁴ W. Zhao, Z. Ghorannevis, K. K. Amara, J. R. Pang, M. Toh, X. Zhang, C. Kloc, P. H. Tan, and G. Eda, *Nanoscale* **5**, 9677 (2013).